Features of calcium hexaaluminate formation in alumina-zirconia ceramics

Nina Cherkasova [a] * [ID], Kristina Antropova [a], Ruslan Kuzmin [a] [ID],
Kemal Emurlaev [ab] [ID], Ivanna Kuchumova [ac], Nomina Burkhinova [a],
Yulia Zobova [a]

a: Novosibirsk State Technical University, Novosibirsk 630073, Russia
b: Synchrotron Radiation Facility SKIF, Boreskov Institute of Catalysis SB RAS, Novosibirsk 630559, Russia
c: Lavrentyev Institute of Hydrodynamics SB RAS, Novosibirsk 630090, Russia
* Corresponding author: cherkasova.2013@corp.nstu.ru

Abstract

Alumina-zirconia composites containing calcium hexaaluminate in the amount from 0 to 15 wt.% were investigated. The materials were obtained by water dispersion, granulation, axial pressing, and free sintering. Density and open porosity were determined by the hydrostatic weighing method. Phase analysis was performed using synchrotron radiation. Structural investigations were conducted using scanning and transmission electron microscopy. Vickers hardness was determined at a load of 10 kg. Fracture toughness was determined by the indentation method. With increasing $CaAl_{12}O_{19}$ content in the composites, the relative density decreased from 98.5% to 91.8%, and the open porosity increased from 0.2 to 1.4%. The lattice parameters of $t-ZrO_2$ crystal lattice did not change up to 12 wt.% $CaAl_{12}O_{19}$, and the degree of tetragonality was 1.435. The degree of tetragonality decreased for the material with 15 wt.% $CaAl_{12}O_{19}$ and reached 1.420. The lattice parameters of $CaAl_{12}O_{19}$ decreased with increasing content. Platelet size increased with increasing calcium hexaaluminate content. For the materials containing up to 9 wt.% $CaAl_{12}O_{19}$, the average length of the platelets was 2 μm, the width was 0.4 μm, and the aspect ratio was 5. For the material with maximum calcium hexaaluminate content, the average length of the platelets was 4.2 μm, the width was 0.6 μm, and the aspect ratio was 7. With increasing $CaAl_{12}O_{19}$ content, the hardness decreased from 1700±25 to 1390±30 Hv, and the critical stress intensity factor increased by 34% to 6.7±0.3 MPa·m$^{1/2}$.

Key findings

- The degree of tetragonality decreased for the material with 15 wt.% $CaAl_{12}O_{19}$ and reached 1.420.
- $CaAl_{12}O_{19}$ content of 15 wt.% is most effective in increasing fracture toughness.
- The deflection mechanism is initiated with calcium hexaaluminate content about 15 wt.%.

1. Introduction

Among other materials, alumina-zirconia composites are characterized by a combination of properties of their constituents: high hardness and wear resistance of Al_2O_3, and high strength and fracture toughness of ZrO_2. The combination of these characteristics, along with their refractory nature (above 1600 °C) and chemical resistance, allows them to be used in furnace linings, screw centrifuge rotors and machine parts. In addition, the dielectric properties, which are more significant for Al_2O_3, make these ceramics suitable for use as substrates in integrated circuits and insulators. Composite ceramic materials based on alumina and zirconia, containing hexaaluminates, are employed in

the manufacturing of cutting tools, joint replacement implants, and other structural products [1–6]. Hexaaluminates have positive effect on the fracture toughness of alumina-zirconia composites [7–10]. The mechanisms behind the improvement in fracture toughness, based on the change in crack propagation trajectory, are effectively realized through the inclusion of elongated grains in the sintered material structure. Such additives include elongated crystals of silicon carbides and nitrides, carbon fibers and platelet structures of hexaaluminates. Presently, research focusing on investigating the structure of hexaaluminate grains and their influence on the phase composition of ceramics is of great interest.

Hexaaluminates are described by the general formulae $MeAl_{11}O_{18}$, $MeAl_{12}O_{19}$, where Me is an alkali or alkaline earth metal. Their structure corresponds to hexagonal symmetry with space group P63/mmc. These compounds have β-Al_2O_3 or magnetoplumbite structures. Both structures consist of layered blocks of $[Al_{11}O_{16}]^+$ spinel separated by $[M^+O]^-$ and $[M^{2+}AlO_3]^-$ mirror planes, correspondingly. The structure depends on the radius and valence of the stabilizing cation. Alkaline oxides form β-Al_2O_3 type structures. Alkaline-earth and rare-earth oxides form magnetolumbites. Divalent cations improve the stabilization of spinel blocks by reducing the number of vacancies in the unit cell. This leads to the formation of a stoichiometric compound [11,12].

Hexaaluminate grains have a platelet structure that provides repeated fracture propagation trajectory changes along them. It is also possible to cut the platelets in the length and width directions. In this case, cleavage proceeds in weakly bound interspinel layers [11].

Calcium hexaaluminate is widely used to increase fracture resistance. $CaAl_{12}O_{19}$ is the only hexaaluminate with a magnetoplumbite structure and a constant stoichiometric formula $MeAl_{12}O_{19}$. In other magnetoplumbites, such as $LaMgAl_{11}O_{19}$, the Me and Al contents can be varied. Thus, research on alumina-zirconia ceramics with $CaAl_{12}O_{19}$ shows the effect of hexaaluminate with magnetoplumbite structure on the phase composition and properties of composites without the contribution of the ratio of Me and Al atoms [11].

Sktani et al. [13] observed an effective fracture toughness improvement at a low additive amount in a material containing 80 wt.% Al_2O_3 and 20 wt.% ZrO_2. Increasing the content of $CaAl_{12}O_{19}$ up to 4 wt.% leads to an increase in the fracture toughness from 5.8 to 6.3 $MPa \cdot m^{1/2}$. $CaAl_{12}O_{19}$ content up to 13 wt.% is associated with a linear decrease in fracture toughness up to 5.5 $MPa \cdot m^{1/2}$. This value is lower than that in the initial material without additives. Similar results were also obtained by other researchers [14–17].

In [9], multi-phase composites based on Al_2O_3 with $CaAl_{12}O_{19}$, $MgAl_2O_4$ and Ni were studied. A blend of CaO- and MgO-based powders was used as the initial material to form hexaaluminate and magnesium aluminate spinel during the sintering process of the composites. It was shown that increasing the amount of the added powders up to 4.89 wt.% increases the fracture toughness from 6 to 6.9 $MPa \cdot m^{1/2}$. With further increase of the additive, the fracture toughness decreases to 5 $MPa \cdot m^{1/2}$. The authors attribute this to a change in the fracture surface morphology at the cracks.

Strontium hexaaluminate, which possesses a structure similar to $CaAl_{12}O_{19}$, exhibits comparable effects on the structure and properties of materials. Several researchers [18–20] reported significant improvement in strength and fracture toughness. However, they found that hardness decreases and porosity increases [19, 21]. In a study by Podzorova et al. [22] the mechanical properties of composites containing 20 mol.% Al_2O_3 and 80 mol.% 3Yb-TZP modified with strontia were investigated. The authors demonstrated that $SrAl_{12}O_{19}$ content exceeding 3% increases porosity. In addition, they discovered that modifying the composite with 1–2 mol.% SrO elevates the flexural strength up to 850 MPa and the fracture toughness up to 11.3 $MPa \cdot m^{1/2}$.

Shi et al [23] showed that alumina ceramics with the addition of 2 mol.% CeO_2 have the highest flexural strength and fracture toughness: 576 MPa and 5.15 $MPa \cdot m^{1/2}$, corresponding to an increase of 21% and 20% compared to the material without additives. These data are in agreement with the results of Liu et al [24].

However, the effects of the content of calcium hexaaluminate on the structure and properties of alumina-zirconia ceramics have been less studied despite the large number of studies in this area. The features of calcium hexaaluminate crystal growth in Al_2O_3-ZrO_2 matrix depending on the content of initial calcium oxide powder have not been revealed.

2. Materials and Methods

Submicron powders of α-Al_2O_3 (Almatis CT 3000 SG, D50 = 0.5 μm), 3Y-ZrO_2 (Stanford Materials, D50 = 0.5 μm) and CaO were used as initial materials. The amount of zirconia in all investigated compositions was 50 wt.%, initial calcia from 0 to 1.26 wt.%, and the remaining was alumina. Calcia was introduced according to the calculation of formation in the sintered materials from 0 to 15 wt.% $CaAl_{12}O_{19}$ with a step of 3%. Water-based suspensions were prepared in a 1:1 ratio by weight. For deagglomeration of the powders, 2 wt.% of Dolapix defloculant was introduced. Before granulation, 1 wt.% of a 10 wt.% solution of grade PVA and 1 wt.% of PEG 400 were introduced.

Suspensions were prepared by dispersion in a ball mill for 24 h. Grinding bodies with a diameter of 0.8 mm were made of zirconia. After evaporating the water from the suspensions, the obtained dry mass was crushed in a ceramic mortar with a ceramic pestle and sieved using a mesh size of 100–250 μm. Granular powders were compacted by axial pressing on an Instron 3369 test machine.

The molding pressure was 100 MPa. Thus, samples in the form of bars were obtained. Pressureless sintering was performed in a tube furnace at 1520 °C for 2 h.

The study of the formed phases was accompanied by the determination of the lattice periods by X-ray diffraction analysis. For this purpose, diffraction patterns were obtained at the Siberian Center for Synchrotron and Terahertz Radiation using a VEPP-4 electron gas booster (Novosibirsk, Institute of Nuclear Physics, Siberian Branch of the Russian Academy of Sciences, channel 8-A, hard X-ray diffraction). Synchrotron X-ray radiation was used as the photon source. The diffraction patterns were registered in the transmission mode using a two-axis Mar354s detector with a pixel size of $100{\times}100$ μm² and a scanning area diameter of 345 mm. Monochromatic radiation was generated using a silicon butterfly-type crystal; the wavelength was 0.178 Å, in a beam size of $200{\times}200$ μm². Circular diffraction patterns were averaged by azimuthal integration using PyFAI software (Python Fast Azimuthal Integration).

To determine the lattice periods, refinement of the diffraction profiles was performed using the pseudo-Voit function combined with a fifth degree polynomial (to estimate the background). The profile analysis allowed us to determine the positions of the X-ray maximum reflections of the studied phases. Then, a redefined system of equations for a defined phase was prepared on the basis of the Wulff–Bragg's equation and solved using the least squares method:

$$\begin{cases} 2d_0 \sin\theta_0 = \lambda \\ 2d_1 \sin\theta_1 = \lambda \\ \quad \dots \\ 2d_n \sin\theta_n = \lambda \end{cases}, \qquad (1)$$

where d_i – interplanar spacing; θ_i – angle corresponding to the interplanar spacing d_i; λ – wavelenght; n – number of analyzed reflections of the studied phase.

Mathematical criterion of diffraction profiles approximation quality was evaluated using R-factor according to the formula:

$$R = \sum_i \frac{|I_e - I_c|}{I_c}, \qquad (2)$$

where I_e – experimental intensity values, I_c – values obtained by calculation.

The phases were identified using the ICDD PDF 4+ database.

The apparent density and open porosity were determined for the sintered samples by hydrostatic weighing. The AD-1653 density determination setup based on the AND GR-300 analytical scale was used. The theoretical density of the composites was calculated. The relative density of the sintered materials under study was estimated. Structural investigations of the samples were performed using a Carl Zeiss EVO 50 scanning electron microscope at magnifications up to x20000. The samples were prepared according to standard technology using diamond suspensions. The samples were etched with concentrated hydrofluoric acid for 10 seconds. The obtained images were processed and analyzed using the JMicroVision software version 1.2.7

[25]. The composites were also investigated by transmission microscopy (TEM) on a JEOL JEM 2100 in STEM mode and using an INCA X-max device for micro X-ray spectral analysis.

Fracture toughness was determined by the indentation method. The tests were performed using an EMCO-TEST DuraScan 50 testing machine. A diamond Vickers pyramid was used as the indenter. The load was 10 kg. At least 5 indents were obtained on each sample.

After the measurements, the values of the critical stress intensity factor were calculated. Calculations were performed according to the Niihara equation, in which the contribution of the Young's modulus of materials is included [26]:

$$K_{Ic} = 0.048 \cdot \left(\frac{c}{a}\right)^{-0.5} \cdot \left(\frac{H_v}{E\varphi}\right)^{-0.4} \cdot \frac{H_v \cdot a^{0.5}}{\varphi}, \mathrm{MPa \cdot m^{1/2}} \qquad (3)$$

where H_v – hardness, GPa; E – Young's modulus, GPa; c – crack length, μm; a – half-diagonal length of an indentation, μm; φ – constraint factor (φ = 3).

3. Results and Discussion

The relative density and open porosity of the investigated materials are shown in Table 1. It was found that an increase in the number of introduced additives decreases the density and increases the porosity of the materials. Although the relative density of the composites decreases significantly with increasing initial CaO additive content, the porosity increases only slightly. For the materials without the CaO additive the porosity was 0.2%, whereas for those containing 15 wt.% $CaAl_{12}O_{19}$ the porosity was 1.4%. In [7], the influence of calcium hexaaluminate at contents of 10 and 15 wt.% on the properties of alumina-zirconia ceramics was studied. At the minimum content of calcium hexaaluminate the authors obtained the material with the highest density; subsequently, porosity began to increase. With the addition of 15 wt.% calcium hexaaluminate, the porosity reached such values that the resulting ceramics can be characterized as porous. The authors also note that the density of $CaAl_{12}O_{19}$ is lower than that of zirconia. Therefore, calcium hexaaluminate is subject to volume expansion, which leads to pore reduction. Nevertheless, the sintering temperature required for such densification is 1750 °C. During cooling from such a high temperature, a large number of monoclinic zirconia phases can form, which negatively affects the mechanical properties. The authors concluded that a lower sintering temperature results in higher grain growth, which can lead to a greater reduction in the number of closed pores, improving the mechanical properties. The platelet shape of $CaAl_{12}O_{19}$ grains inhibits the diffusion and sintering processes, promotes the formation of intergranular porosity, and, consequently, increases the open porosity of the material [27].

The investigations were conducted using X-ray phase analysis. The results are shown in Figure 1. Two phases

are present in the material without additives: α-Al_2O_3 and t-ZrO_2. The introduction of calcia into the matrix led to the formation of calcium hexaaluminate in all compositions studied. At the same time, the m-ZrO_2 phase appeared in such materials. It is probably related to the increase in porosity of the investigated systems and the phase transition of tetragonal to monoclinic 3Y-ZrO_2. This occurs due to the absence of compressive stresses on the matrix grains.

The parameters of the crystal lattices of the main phases in the investigated materials were determined using the method of least squares. The results are presented in Table 2. The studies were carried out for alumina-zirconia ceramics without additives, as well as with 12 and 15 wt.% $CaAl_{12}O_{19}$. It was found that up to 12 wt.% $CaAl_{12}O_{19}$, the lattice parameters of t-ZrO_2 remain unchanged, with a degree of tetragonality equal to 1.435. However, for the material with 15 wt.% $CaAl_{12}O_{19}$, the degree of tetragonality decreased to 1.420. This decrease indicates the dissolution of Ca^{2+} cations in the crystal lattice of t-ZrO_2, which is stabilized by 3 mol.% Y_2O_3.

Therefore, some calcium cations interacted with zirconia but not with Al_2O_3. As a consequence, the parameters of the crystal lattice of $CaAl_{12}O_{19}$ decreased.

Microstructural investigations using scanning electron microscopy were performed. Typical structures are shown in Figure 2. Two types of grains were recorded: dark gray, predominantly equiaxed, Al_2O_3 grains and light ZrO_2 grains. The average grain size for Al_2O_3 is about 1 µm at the 3 wt.% $CaAl_{12}O_{19}$ content, and in areas of its concentration the grain size is 1.67 µm. Then, when the amount of calcium hexaaluminate was increased to 12 wt.%, the average grain size decreased to 0.94 µm. This is due to the formation of $CaAl_{12}O_{19}$. CaO interacts with Al_2O_3 grains to form hexaaluminate during the sintering process. Localized concentrations of Al_2O_3 grains are observed.

A similar dependence was found for zirconia grains. The grain size decreased from 0.43 µm to 0.38 µm with increasing calcium hexaaluminate content from 3 wt.% to 12 wt.%.

The presence of platelets, which are probably $CaAl_{12}O_{19}$ compounds, was detected. The platelet size increased with a higher content of calcium hexaaluminate. For materials containing up to 9 wt.% $CaAl_{12}O_{19}$, the average length of the platelets is 2 µm, with a width of 0.4 µm, resulting in an aspect ratio of 5 (Figure 2a). In the material with the maximum content of calcium hexaaluminate, the average platelet size is about 4.2 µm, the width is 0.6 µm, and the aspect ratio is 7.

Table 1 Relative density and open porosity of sintered materials.

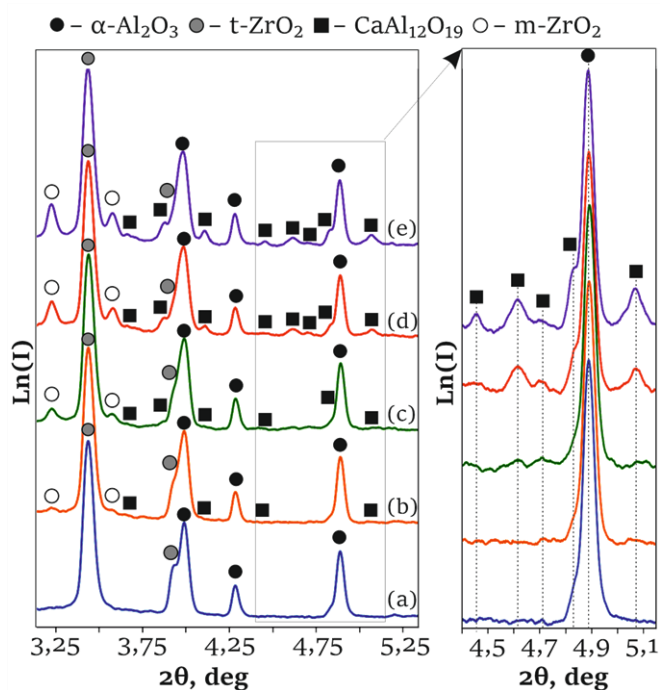| $CaAl_{12}O_{19}$ content, wt.%	Relative density, %	Apparent porosity, %
0	98.5±0.3	0.2±0.1
3	96.3±0.4	0.5±0.1
6	95.0±0.3	0.9±0.2
9	94.4±0.3	0.9±0.2
12	93.2±0.4	1.0±0.2
15	91.8±0.4	1.4±0.3

Table 2 Crystal lattice parameters of the studied materials.

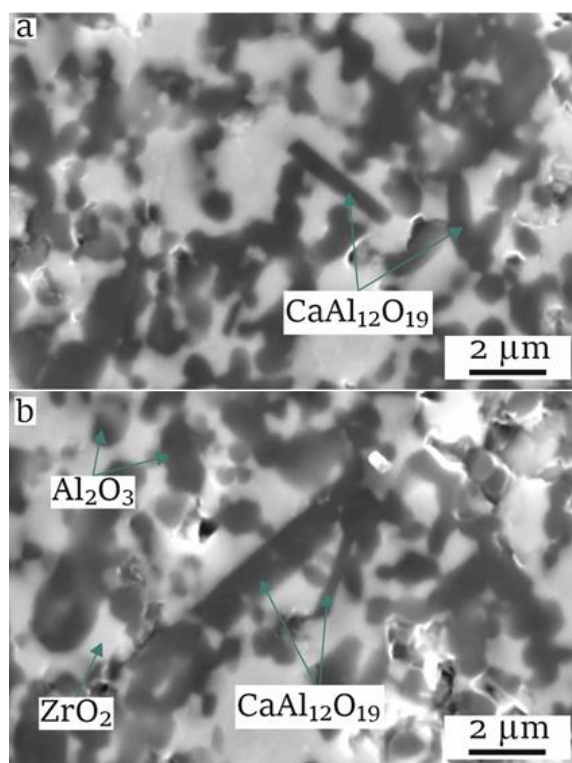| $CaAl_{12}O_{19}$ content, wt.%	α-Al_2O_3	t-ZrO_2	$CaAl_{12}O_{19}$
0 (R = 2.0%)	$a = b$ = 4.775	$a = b$ = 3.618	–
12 (R = 1.1%)	$a = b$ = 4.778	$a = b$ = 3.618	$a = b$ = 5.550
15 (R = 2.3%)	$a = b$ = 4.775	$a = b$ = 3.631	$a = b$ = 5.544

Figure 1 X-ray phase analysis of sintered materials: material without additives (a), with 3 wt.% $CaAl_{12}O_{19}$ (b), with 6 wt.% $CaAl_{12}O_{19}$ (c), with 12 wt.% $CaAl_{12}O_{19}$ (d), with 15 wt.% $CaAl_{12}O_{19}$.(e).

Figure 2 Structure of alumina-zirconia ceramics containing 6 wt.% $CaAl_{12}O_{19}$ (a) и 15 wt.% $CaAl_{12}O_{19}$ (b).

Furthermore, individual platelets up to 6 μm in length were observed (Figure 2b). Therefore, it was found that an increase in CaO content not only leads to an increase in the calcium hexaaluminate content, but also to an increase in the platelet size.

To determine the elemental composition of the fixed platelets, studies by transmission electron microscopy were carried out (Figure 3). Elemental analysis of the platelets showed that they comprised Al, O and Ca. Thus, based on the TEM data and X-ray phase analysis, it was established that the platelets are calcium hexaaluminate.

The hardness and fracture toughness were measured using the indentation method. The results are shown in Table 3. The hardness decreases with increasing $CaAl_{12}O_{19}$ content, which is due to the decrease in alumina content and the increase in porosity in the composites. Similar effects were described in some studies [28–30]. In the sintered material with a minimum $CaAl_{12}O_{19}$ content, the critical stress intensity factor increases by 14%. This is due to the formation of $CaAl_{12}O_{19}$ platelets and the realization of different mechanisms of increasing fracture toughness, such as platelet fracture, bridge formation, and bending mechanism [31, 32]. With further growth of the $CaAl_{12}O_{19}$ content, the critical stress intensity factor decreases. This is probably due to the increase in porosity of the material and its negative contribution to the fracture toughness of the composites. However, at the maximum $CaAl_{12}O_{19}$ content, K_{IC} increases to a maximum value of 6.7±0.3 MPa·m$^{1/2}$. This value is 34% higher than that for the material without additives.
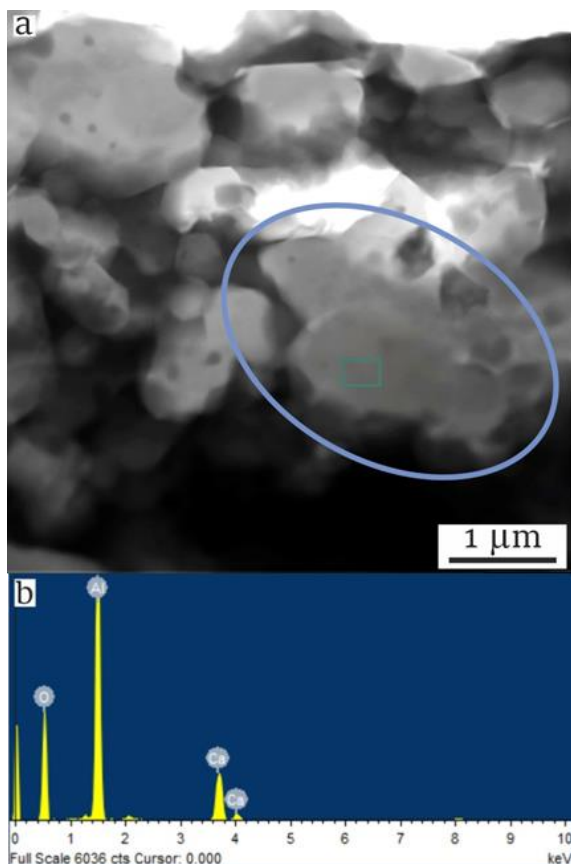
Structural investigations of the crack propagation trajectory in the composites showed that the crack deflection mechanism was realized only in the material with 15 wt.% $CaAl_{12}O_{19}$. An example is shown in Figure 4. Black arrows indicate calcium hexaaluminate platelets, and ovals indicate the areas of crack deflection from the original trajectory. The direction of crack propagation is indicated by green arrows. Thus, the contribution of the crack deflection mechanism has a significant effect on the improvement of fracture toughness. Simultaneously, the negative effect of porosity was eliminated. In addition, it was found that in the material with 15 wt.% $CaAl_{12}O_{19}$ platelet size increased significantly compared with that in the other materials studied.

Earlier, in a study on the effect of strontium hexaaluminate content on the properties of alumina-zirconia ceramics, the effect of crack propagation trajectory deflection was also recorded only in the material with 15 wt.% hexaaluminate [33]. However, main distinctive the feature of that study is the nonlinear change in the critical stress intensity factor with changing calcium hexaaluminate content. This may be associated in part with the nonuniform distribution of $CaAl_{12}O_{19}$ platelets in the structure of the composites. This is explained by the thickening of the water suspensions with increasing CaO content and is described in the paper [34].

4. Limitations

During the investigation, it was difficult to analyze the influence of the structure on the properties of the materials. This is due to the presence of pores and the local nonuniform distribution of calcium hexaaluminate in the materials.

Table 3 Hardness and fracture toughness of ceramic composites.

| $CaAl_{12}O_{19}$ content, wt. %	$H_{v\ 10}$	K_{IC}, MPa·m$^{1/2}$
0	1700±25	5.0±0.2
3	1650±50	5.7±0.2
6	1610±45	5.6±0.3
9	1540±25	5.4±0.2
12	1410±40	5.5±0.2
15	1390±30	6.7±0.3

Figure 3 TEM image of alumina-zirconia ceramics containing 15 wt.% $CaAl_{12}O_{19}$: structure (a), EDS analysis results (b).

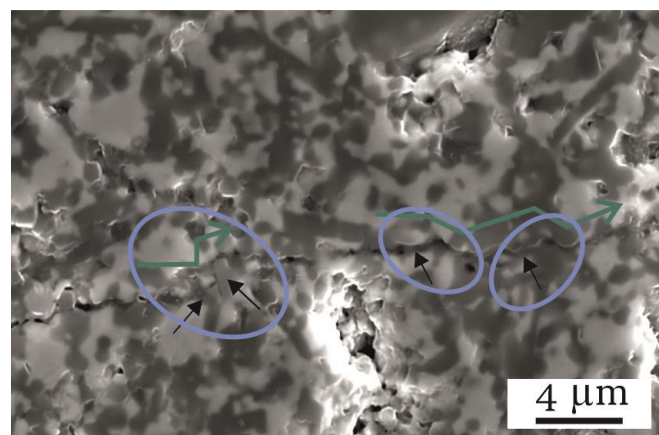**Figure 4** Crack propagation in alumina-zirconia ceramics with 15 wt.% $CaAl_{12}O_{19}$.

The presence of calcium hexaaluminate platelets is associated with an increase in the viscosity of the water suspensions prepared for dispersion. Thus, to improve the mechanical properties of composites with $CaAl_{12}O_{19}$, it is recommended to change the synthesis method. For example, the preparation of alcohol suspensions using hot pressing and spark plasma sintering may be attempted.

5. Conclusions

Our main conclusions are as follows:

1. Introduction of CaO at the dispersion stage leads to the formation of calcium hexaalmuinate in sintered alumina-zirconia ceramics.

2. With increasing content of calcium hexaaluminate in the composites, the relative density decreases to 91.8%, and the porosity increases 7 times.

3. The crystal lattice parameters of the main phases in the investigated materials were determined. Up to 12 wt.% $CaAl_{12}O_{19}$ the lattice parameters of t-ZrO_2 do not change, and the degree of tetragonality is 1.435. For the material with 15 wt.% $CaAl_{12}O_{19}$, the degree of tetragonality decreases to 1.420. The lattice parameters of $CaAl_{12}O_{19}$ decrease with increasing content.

4. Platelet size increases with increasing calcium hexaaluminate content. For materials containing up to 9 wt.% $CaAl_{12}O_{19}$, the average length of the platelets is 2 μm, the width is 0.4 μm, and the aspect ratio is 5. For the material with the maximum content of calcium hexaaluminate, the average length of the platelets is 4.2 μm, the width is 0.6 μm, and the aspect ratio is 7.

5. Formation of 15 wt.% $CaAl_{12}O_{19}$ in alumina-zirconia ceramics increases the critical stress intensity factor by 34% compared with the composite without additives. The deflection mechanism is initiated with calcium hexaaluminate content of approximately 15 wt.%.

● Supplementary materials

No supplementary materials are available.

● Funding

● Acknowledgments

● Author contributions

Conceptualization: N.Ch., K.A.
Data curation: R.K.
Investigation: K.E., I.K., N.B.
Methodology: R.K., R.Kh.
Validation: N.Ch., K.A.
Visualization: Yu.Z.
Writing – original draft: N.Ch., K.A., R.K.

● Conflict of interest

The authors declare no conflict of interest.

● Additional information

Author IDs:
Nina Cherkasova Scopus ID 56971176200;
Kristina Antropova Scopus ID 57759105600;
Ruslan Kuzmin, Scopus ID 57189894268;
Kemal Emurlayev Scopus ID 57189889192;
Ivanna Kuchumova, Scopus ID 57202436655;
Nomina Burkhinova, Scopus ID 57886417900.

Websites:
Novosibirsk State Technical University, https://en.nstu.ru/;
Boreskov Institute of Catalysis SB RAS, https://en.catalysis.ru/;
Lavrentyev Institute of Hydrodynamics SB RAS, http://www.hydro.nsc.ru/.

References

1. Yıldız BK, Tür YK. Effect of ZrO_2 content on the microstructure and flexural strength of Al_2O_3–ZrO_2 composites with the stored failure energy-fragmentation relations. Ceram Int. 2021;47(24):34199–34206. doi:10.1016/j.ceramint.2021.08.329

2. Anjaneyulu B, Nagamalleswara Rao G, Prahlada Rao K. Development, mechanical and tribological characterization of Al_2O_3 reinforced ZrO_2 ceramic composites. Mater Today Proc. 2021;37:584–591. doi:10.1016/j.matpr.2020.05.594

3. Smuk B, Szutkowska M, Walter J. Alumina ceramics with partially stabilized zirconia for cutting tools. J Mater Process Technol. 2003;133(1–2):195–198. doi:10.1016/S0924-0136(02)00232-7

4. Kern F, Gadow R. In Situ Platelet Reinforcement of Alumina and Zirconia Matrix Nanocomposites – One Concept, Different Reinforcement Mechanisms. Adv Sci Technol. 2014;87:118–125. doi:10.4028/www.scientific.net/AST.87.118

5. Fornabaio M, Palmero P, Traverso R, Esnouf C, Reveron H, Chevalier J, Montanaro L. Zirconia-based composites for biomedical applications: Role of second phases on composition, microstructure and zirconia transformability. J Eur Ceram Soc. 2015;35(14):4039–4049. doi:10.1016/j.jeurceramsoc.2015.04.027

6. Piconi C, Maccauro G, Muratori F, Prever EB Del. Alumina and zirconia ceramics in joint replacements. J Appl Biomater Funct Mater. 2003;1(1):19–32. doi:10.1177/228080000300100103

7. Chen Z, Chawla K., Koopman M. Microstructure and mechanical properties of in situ synthesized alumina/Ba-β-alumina/zirconia composites. Mater Sci Eng A. 2004;367(1–2):24–32. doi:10.1016/j.msea.2003.09.070

8. Kern F, Gommeringer A. Reinforcement Mechanisms in yttria-ceria-co-stabilized zirconia- alumina-strontium hexaaluminate composite ceramics. J Ceram Sci Technol 2018;98:93–98. doi:10.4416/JCST2017-00046

9. Zhang X, Liang J, Li J, Zeng Y, Hao S, Liu P, Na H. The properties characterization and strengthening-toughening mechanism of Al_2O_3-CA6-MA-Ni multi-phase composites prepared by adding calcined dolomite. Mater Charact. 2022;186:111810. doi:10.1016/J.MATCHAR.2022.111810

10. Sirotinkin V, Podzorova L, Il'icheva A. Comparative X-ray diffraction study of the Yb_2O_3 stabilized zirconia ceramics doped with SrO and CaO. Mater Chem Phys. 2022;277:125496. doi:10.1016/J.MATCHEMPHYS.2021.125496

11. Cinibulk MK. Hexaluminates as a cleavable fiber–matrix interphase: synthesis, texture development, and phase compatibility. J Eur Ceram Soc. 2000;20(5):569–582. doi:10.1016/S0955-2219(99)00255-1

12. Tian M, Wang XD, Zhang T. Hexaaluminates: a review of the structure, synthesis and catalytic performance. Catal Sci Technol. 2016;6(7):1984–2004. doi:10.1039/C5CY02077H

13. Sktani ZDI, Azhar AZA, Ratnam MM, Ahmad ZA. The influence of in-situ formation of hibonite on the properties of zirconia toughened alumina (ZTA) composites. Ceram Int. 2014;40(4):6211–6217. doi:10.1016/j.ceramint.2013.11.076

14. Nagaoka T, Yasuoka M, Hirao K, Kanzaki S, Yamaoka Y. Effects of CaO addition on sintering and mechanical properties of Al_2O_3. J Mater Sci Lett. 1996;15(20):1815–1817. doi:10.1007/BF00275351

15. Asmi D, Low IM, O'Connor BH. Physical, thermal, and mechanical properties of Al_2O_3-$CaAl_{12}O_{19}$ composites processed by in-situ reaction sintering. J Sains MIPA Univ Lampung. 2012;4(1):1–8.

16. Podzorova LI, Il'icheva AA, Pen'kova OI, Antonova OS, Baikin AS, Konovalov AA. Al_2O_3-based ceramic composites with a high brittle fracture resistance. Inorg Mater. 2019;55(6):628–33. doi:10.1134/S0020168519060128

17. Ismail H, Mohamad H. Effects of $CaCO_3$ additive on the phase, physical, mechanical, and microstructural properties of zirconia-toughened alumina-CeO_2-Nb_2O_5 ceramics. Ceram Int. 2023;49(22):36850–36856. doi:10.1016/j.ceramint.2023.09.015

18. Burger W, Richter HG. High Strength and Toughness Alumina Matrix Composites by Transformation Toughening and «In Situ» Platelet Reinforcement (ZPTA) – The New Generation of Bioceramics. Key Eng Mater. 2000;192–195:545–548. doi:10.4028/www.scientific.net/KEM.192-195.545

19. Naga SM, Elshaer M, Awaad M, Amer AA. Strontium hexaaluminate/ZTA composites: Preparation and characterization. Mater Chem Phys. 2019;232:23–27. doi:10.1016/j.matchemphys.2019.04.055

20. Arab A, Ahmad R, Ahmad ZA. Effect of $SrCO_3$ addition on the dynamic compressive strength of ZTA. Int J Miner Metall Mater. 2016;23(4):481–489. doi:10.1007/s12613-016-1259-3

21. Vishista K, Gnanam FD. Effect of strontia on the densification and mechanical properties of sol–gel alumina. Ceram Int. 2006;32(8):917–922. doi:10.1016/J.CERAMINT.2005.06.014

22. Podzorova LI, Il'icheva AA, Sirotinkin VP, Antonova OS, Baikin AS, Kutuzova VE, Pen'kova OI. Ceramic composites of the zirconium dioxide and aluminum oxide system including strontium hexaaluminate. Glas Ceram (English Transl Steklo i Keramika). 2021;78(5–6):231–236. doi:10.1007/S10717-021-00385-X

23. Shi S, Cho S, Goto T, Sekino T. Role of $CeAl_{11}O_{18}$ in reinforcing Al_2O_3/Ti composites by adding CeO_2. Int J Appl Ceram Technol. 2021;18(1):170–181. doi:10.1111/ijac.13629

24. Liu M, Wang Z, Luan X, Wu J, Li Q. Effects of CeO_2 and Y_2O_3 on the interfacial diffusion of Ti/Al_2O_3 composites. J Alloys Compd. 2016;656:929–935. doi:10.1016/j.jallcom.2015.10.043

25. Roduit N. JMicroVision: Image analysis toolbox for measuring and quantifying components of high-definition images. Version 1.3.4.

26. Niihara K, Morena R, Hasselman DPH. Evaluation of K_{Ic} of brittle solids by the indentation method with low crack-to-indent ratios. J Mater Sci Lett. 1982;1(1):13–16. doi:10.1007/BF00724706

27. Cui S, Wang Q, Zhou Y, Mao D, Bao J, Song X. Effect of nickel oxide and titanium oxide on the microstructural, optical, and mechanical properties of calcium hexaaluminate ceramics. Ceram Int. 2021;47(24):35302–35311. doi:10.1016/j.ceramint.2021.09.073

28. Cherkasova NY, Bataev AA, Veselov SV, Kuzmin RI, Stukacheva NS, Zimogliadova TA. Structure and fracture toughness of ceramics based on Al_2O_3 and ZrO_2 with $SrAl_{12}O_{19}$ additive. Lett Mater. 2019;9(2). doi:10.22226/2410-3535-2019-2-179-184

29. Suzuki Y, Nishihashi K. Microstructures and mechanical properties of reactively sintered $CaAl_{12}O_{19}$/$CaAl_4O_7$ porous composites. Ceram Int. 2023;49(18):29427–29432. doi:10.1016/j.ceramint.2023.06.004

30. Zhang X, Zeng Y, Liang J, Li J, Hao S, Wang Y. The microstructure and mechanical properties of Ni/Al_2O_3 composites by in-situ generated $CaAl_{12}O_{19}$ and ZrO_2 via hot pressing sintering. Ceram Int. 2020;46(9):13144–13150. doi:10.1016/j.ceramint.2020.02.088

31. Gogotsi GA. Fracture toughness of ceramics and ceramic composites. Ceram Int. 2003;29(7):777–784. doi:10.1016/S0272-8842(02)00230-4

32. Evans AG, Charles EA. Fracture toughness determinations by indentation. J Am Ceram Soc. 1976;59(7–8):371–372. doi:10.1111/j.1151-2916.1976.tb10991.x

33. Cherkasova N, Kuzmin R, Veselov S, Antropova K, Ruktuev A, Ogneva T, Tyurin A, Kuchumova I, Khabirov R. Influence of strontium hexaaluminate percentage on the structure and properties of alumina-zirconia ceramics. Mater Chem Phys. 2022;288:126424. doi:10.1016/j.matchemphys.2022.126424

34. Cherkasova NY, Kuz'min RI, Antropova KA, Burkhinova NY. Rheological characteristics of suspensions and structure of Al_2O_3–CaO and Al_2O_3–SrO composites. Refract Ind Ceram. 2022;63(3):311–314. doi:10.1007/s11148-022-00727-4